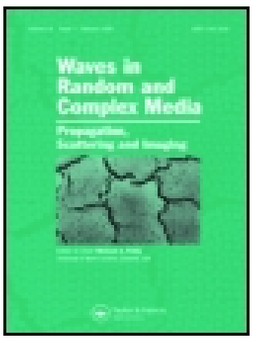

Waves in Random and Complex Media

ISSN: (Print) (Online) Journal homepage: https://www.tandfonline.com/loi/twrm20

Optimal absorption of flexural energy in thin plates by critically coupling a locally resonant grating

J. Leng, V. Romero-García, F. Gautier, A. Pelat, R. Picó & J.-P. Groby

To cite this article: J. Leng, V. Romero-García, F. Gautier, A. Pelat, R. Picó & J.-P. Groby (2021): Optimal absorption of flexural energy in thin plates by critically coupling a locally resonant grating, Waves in Random and Complex Media, DOI: 10.1080/17455030.2021.1930278

To link to this article: https://doi.org/10.1080/17455030.2021.1930278

WAVES IN RANDOM AND COMPLEX MEDIA
https://doi.org/10.1080/17455030.2021.1930278

Taylor & Francis
Taylor & Francis Group

Optimal absorption of flexural energy in thin plates by critically coupling a locally resonant grating

J. Leng[a], V. Romero-García[a], F. Gautier[a], A. Pelat[a], R. Picó[b] and J.-P. Groby[a]

[a]Laboratoire d'Acoustique de l'Université du Mans (LAUM), UMR CNRS Institut d'Acoustique - Graduate School (IA-GS), CNRS, Le Mans Université, Le Mans, France; [b]Instituto para la Gestión Integral de zonas Costeras (IGIC), Universitat Politècnica de València, Gandia, Spain

ABSTRACT

The optimal absorption of flexural energy by the critical coupling of a locally resonant grating embedded in a thin plate is reported in this work for the reflection and transmission problems. The grating is made of a 1D-periodic array of local resonators. A viscoelastic coating is also placed on top of each resonator to control the intrinsic losses of the system. The scattering matrices for the propagative waves of both problems are obtained by means of the Layered Multiple Scattering Theory and validated by the Finite Element Method. In this work, we find that the perfect absorption can be obtained in the reflection problem and the maximal absorption in the transmission problem is limited to 50% by tuning the losses only. These results agree with the theoretical predictions since the eigenvalues reduce to the reflection coefficient in the reflection problem and only one of the two eigenvalues of the scattering matrix is critically coupled in the transmission problem. These results highlight the adaptability of the critical coupling method to optimize the absorption of locally resonant materials for flexural waves in 2D transmission and reflection problems, and pave the way to the design of resonators for efficient flexural wave absorption.

ARTICLE HISTORY
Received 25 October 2020
Accepted 10 May 2021

KEYWORDS
Flexural Waves; Perfect Absorption; Multiple Scattering; Metamaterials; Critical Coupling

1. Introduction

Mitigation of low-frequency vibrations in plates by small and lightweight systems is a crucial issue, especially in transport engineering where weight and space concerns remain critical. While usual current passive methods for vibration control lead to heavy and bulky solutions by making use of viscoelastic materials [1] or Tuned Vibration Absorbers (TVA) [2], other solutions relying on Locally Resonant Materials (LRMs), i.e. metamaterials, have emerged over the past decades [3,4].

LRMs are made of resonant building blocks embedded in a host medium. The distribution of these blocks usually follows a periodic pattern in such a way that the wavelength corresponding to their resonance frequency is much larger than the periodicity of the system. This results in a resonance frequency that is much lower than the Bragg frequency

CONTACT J. Leng julien.leng@univ-lemans.fr

and a strong dispersion in the LRMs around the resonance frequency, leading to original features and properties in the deep subwavelength regime, i.e. with dimensions that are much smaller than the wavelength of the impinging propagating waves. These properties are exploited in particular in vibration control from wave filtering and focusing to waveguiding, among others [5–12]. However, among all the possibilities offered by LRMs for flexural waves, very few studies have focused on maximizing the flexural wave absorption at low frequencies with small and lightweight systems. In this context, subwavelength perfect absorbers, which have been extensively studied in acoustics and electromagnetism [13–16], are of particular interest for vibration damping. These absorbers have been recently proposed for 1D resonant beam systems, demonstrating the possibility to perfectly absorb the energy of one dimensional flexural waves [17].

Subwavelength perfect absorbers provide a total absorption of incident wave energy whose wavelength is much larger than the size of the absorbers [18–23]. Their scattering process for propagative waves can be represented in general by the scattering matrix. In terms of this matrix, the perfect absorption appears at the frequencies at which its eigenvalues are zero. This is known as the critical coupling condition or simply impedance matching condition. From a physical point of view, this critical coupling condition is obtained by making use of two properties of the perfect absorber. First, the field inside the resonator interacts with the external one (i.e. with that in the surrounding medium) through the interface that connects the absorber to the medium. The wave energy can leak out through this connection from the absorber to the surrounding medium and vice-versa. The absorber is thus open to the surrounding medium and the quality factor of its resonance represents its energy leakage. Second, the inherent losses of the resonator are accounted for and form an internal source of energy dissipation. The critical coupling of such resonant absorbers is controlled by the ratio between the inherent losses and the energy leakage [24]. Particularly, this corresponds to the situation in which the inherent losses exactly compensate the energy leakage, i.e. when intrinsic losses are the same as the energy leakage [25]. This situation leads to a maximal absorption of the wave energy [15,17]. Such a physical phenomenon has been broadly studied in various fields for the reflection problem [26,27]. However, less attention has been paid in maximizing the absorption in a transmission problem, where the critical coupling conditions are more difficult to obtain.

This work analyzes the scattering of flexural waves by an infinite critically coupled grating made of local and identical resonators embedded in a thin plate. The local resonators are made of circular reductions of the plate thickness in the center of which a mass is added. A viscoelastic layer is also placed on top of each resonator to control the intrinsic losses of the system. More specifically, this work focuses on the analysis of the absorbing efficiency of this locally resonant grating in two configurations. The first one corresponds to a transmission problem in which the grating is excited by a plane wave and the reflection and transmission properties are evaluated to obtain the absorption. The second corresponds to a reflection problem in which the scattered field by the grating interacts with a simply supported boundary in a semi-infinite thin plate. This boundary is also assumed to be parallel to the grating axis. The excitation in both configurations takes the form of an incident plane wave and is normal to the grating axis. The dimensions of the system are chosen in such a way that the first resonance frequency of the inclusions are three times smaller than the Bragg frequency of the grating. With these dimensions, the local resonances are well decoupled to the Bragg diffraction of the grating and only the resonance is playing a role

in the absorption process. The case in which the resonance frequency is close to the Bragg frequency is also analyzed in order to show that perfect absorption can also be achieved with several resonances playing a role in the absorption process. The composite material formed by the inclusion and the viscoelastic coating is analytically modeled with the Ross–Kerwin–Ungar (RKU) model for plates [1] and its losses are tuned in order to optimize the absorption coefficient in both configurations.

The scattered field by the grating is studied by means of Layered Multiple Scattering Theory (LMST) [28–31], which is perfectly adapted to the study of wave propagation in LRMs. Other numerical and analytical theories developed over the past decades also lend themselves to this type of study. Examples of such theories include the plane-wave expansion (PWE) method, finite-difference time-domain (FDTD) method, finite element method (FEM), and multiple scattering theory (MST) [31,32]. The results obtained from LMST in this work are also numerically validated using a 3D semi-periodic FEM model from solid mechanics in COMSOL Multiphysics®. The key feature of LMST is the application of field identities called lattice sums or Schlömilch series [33] that makes use of Graf's addition theorem [34] and Bloch–Floquet condition to relate the scattered displacement field in the vicinity of one scatterer to the fields scattered by all the others and arising from the external sources. The main difficulty in the evaluation of these identities arises through their conditional convergence due to the presence of Hankel function in the solution. Various works have been devoted to the development of efficient and accurate methods for their calculation [35,36] since Twersky's seminal work [37]. Although MST or LMST have been widely implemented in vibration for waveguiding, wave focusing and filtering [5,9–11,38–42], its implementation for maximizing the flexural wave absorption at low frequencies by using local resonances have not been proposed in previous works.

The article is organized as follows. The formulation of the problems is presented in Section 2. Section 3 summarizes the LMST as the semi-analytical model used to study the scattering properties of the infinite grating made of the local resonators coated by a viscoelastic layer and embedded in a thin plate. Section 4 presents and discusses the critically coupled transmission and reflection problems. Section 4.3 also presents an alternative optimization of the absorption by making use of the local resonances and the periodicity of the grating in the case of platonic crystal, i.e. when the first resonance frequency of the inclusions are close to the Bragg frequency of the grating. Finally, Section 5 outlines the main results and gives the concluding remarks.

2. Formulation of the problem

This section aims at describing the two configurations of scattering problems analyzed in this work and also defining the theoretical context by means of the flexural wave equation and the incident wave definitions.

2.1. Description of the configurations

2.1.1. Transmission and reflection problem

The two configurations analyzed in this work are represented in Figure 1, which represents two views of an infinite thin plate in which a locally resonant grating is embedded. The thin host plate has a constant thickness h, Young's modulus E, Poisson's ratio ν, mass density ρ

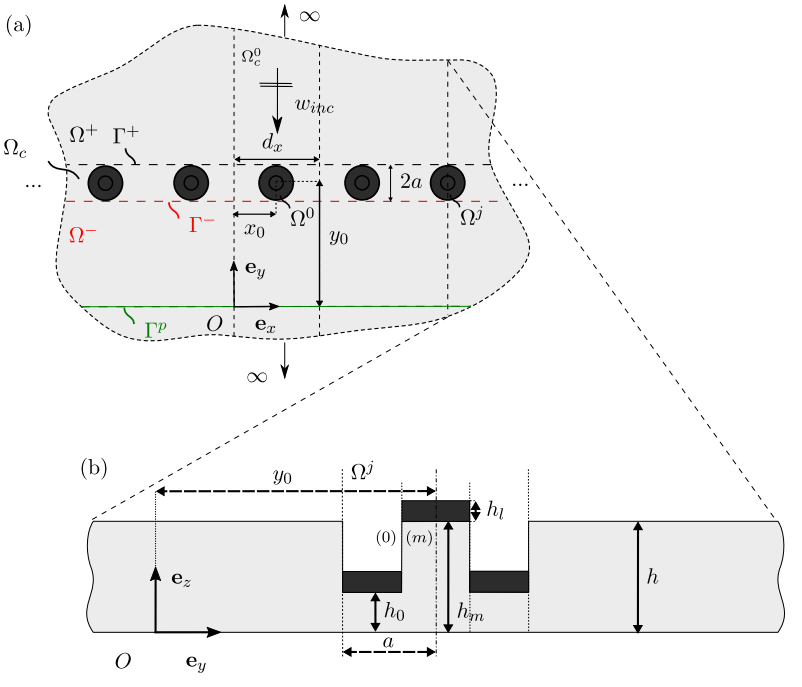

Figure 1. (a) Scheme of the transmission problem by an infinite grating of circular inclusions embedded in a thin plate. The configuration of the reflection problem is obtained by substituting the interface Γ^- by the interface Γ^p in which a simply supported condition is considered. (b) Side view of the unit cell Ω_c^j.

and flexural rigidity $D = \frac{Eh^3}{12(1-\nu^2)}$. The first configuration corresponds to what is named in this work as the transmission problem, in which the locally resonant grating is embedded in an infinite thin plate and excited by an incident plane wave as indicated in Figure 1(a). The grating is limited between the interfaces Γ^+ and Γ^- as shown in Figure 1(a). The goal of the study of this first configuration consists in evaluating the reflection and transmission coefficients produced by the grating and making the connection between the performance of the system with the critical coupling conditions in order to evaluate the limits of absorption. The second configuration corresponds to what is named as the reflection problem, in which the locally reacting grating is placed in front of a simply supported boundary as indicated in Figure 1(a). This boundary corresponds to the interface Γ_p placed at a distance y_0 from the center of the grating and parallel to its axis. The system is also excited by a plane wave and the scattered field is produced by a multiple scattering process between the inclusions and the simply supported boundary.

2.1.2. Unit cells

Due to the periodicity of the system along the $\mathbf{e}_x$-axis, a semi-infinite unit cell Ω_c^0 of width d_x is considered in both configurations. This unit cell is attached to a global Cartesian coordinate system $(O, \mathbf{e}_x, \mathbf{e}_y)$, and thus the position vector is written as $\mathbf{x} = x\mathbf{e}_x + y\mathbf{e}_y$. The analyzed system consists of the d_x-periodic repetition of the unit cell Ω_c^0 along the direction

$\mathbf{e}_x$. The jth repetition of the unit cell is denoted Ω_c^j where $j \in \mathbb{Z}$, and is included in the Cartesian domain $x \in [0 + jd_x; d_x + jd_x]$ and $y \in [y_0 - a; y_0 + a]$ for the transmission problem, and $x \in [0 + jd_x; d_x + jd_x]$ and $y \in [0; y_0 + a]$ for the reflection problem.

2.1.3. Inclusions

A circular inclusion of radius a and denoted by Ω^0 is placed in the unit cell Ω_c^0. The inclusion consists of a circular reduction of the plate thickness with a thickness h_0 ($h_0 < h$), in the center of which an added mass of radius a_m and thickness h_m is placed (see the side view of Figure 1(b)). This mass is obtained by locally increasing the thickness of the inclusion ($h_m > h_0$) and is therefore also made of the same material as the host plate. The center of Ω^0 is located at the point $\mathbf{x}_0$ of coordinates $\mathbf{x}_0 = x_0\mathbf{e}_x + y_0\mathbf{e}_y = d_x/2\mathbf{e}_x + y_0\mathbf{e}_y$ (see Figure 1(a)). The inclusion is coated by a viscoelastic layer of constant thickness h_l as shown in Figure 1(b), whose material properties are defined by Young's modulus E_l, Poisson's ratio ν_l, density ρ_l and loss factor η_l. Each inclusion can be discretized in two homogeneous axisymmetric layers, one containing the added mass and denoted by (m), and another without mass denoted by (0) (see Figure 1(b)). The boundary conditions at the interfaces between layer (m) and (0), and layer (0) and the surrounding plate, are the continuity of the displacement, the normal derivative of the displacement, the bending moment and the (Kirchhoff) shear force.

2.1.4. Domains Ω_c, Ω^+ and Ω^-

In the first configuration corresponding to the transmission problem, the d_x-periodic repetition of Ω_c^0 can be divided into three domains Ω_c, Ω^+ and Ω^- (see Figure 1(a)) where

- Ω_c corresponds to the grating of d_x-periodic repetitions of Ω^0 and is included in the Cartesian domain $x \in [-\infty; +\infty]$ and $y \in [y_0 - a; y_0 + a]$,
- Ω^+ corresponds to the upper half-space included in the domain $x \in [-\infty; +\infty]$ and $y \in [y_0 + a; +\infty]$, where the incident wave initially propagates and is reflected from the grating,
- Ω^- corresponds to the lower half-space included in the domain $x \in [-\infty; +\infty]$ and $y \in [-\infty; y_0 - a]$, where the transmitted waves propagate away from the grating.

The interfaces between Ω_c and $\Omega^\pm$ are, respectively, denoted by $\Gamma^\pm$. In the second configuration corresponding to the reflection problem, only Ω^+ is considered since a simply supported boundary is placed below the grating (see Figure 1(a)). The interface between Ω^+ and Ω_c is then denoted Γ^+ in this case, whereas the simply supported boundary is denoted by Γ^p.

2.2. Flexural wave equation and incident wave

Assuming Kirchhoff–Love conditions, the flexural displacement at any position $\mathbf{x}$ in the thin plate satisfies the biharmonic equation of motion [43]:

$$D\nabla^2\nabla^2 W(\mathbf{x}, t) + \rho h \frac{\partial^2 W(\mathbf{x}, t)}{\partial t^2} = 0. \tag{1}$$

This equation can be expressed in the harmonic domain with the time convention $W(\mathbf{x},t) = w(\mathbf{x})\,\mathrm{e}^{-\mathrm{i}\omega t}$ (ω being the angular frequency) as

$$(\nabla^2\nabla^2 - k^4)w(\mathbf{x}) = 0, \tag{2}$$

with $k^4 = \frac{\rho h\omega^2}{D}$, k being the wavenumber. The solution of Equation (2) can be written as the sum of an incident wave w_{inc} and the scattered field w_{sc}:

$$w(\mathbf{x}) = w_{\mathrm{inc}}(\mathbf{x}) + w_{\mathrm{sc}}(\mathbf{x}). \tag{3}$$

The incident field w_{inc} is considered in both problems as a propagative plane wave of unitary amplitude and frequency $f = \frac{\omega}{2\pi}$. Note that w_{inc} initially propagates in Ω^+ with an incident angle which is normal to the grating, and can be written as

$$w_{\mathrm{inc}}(\mathbf{x}) = \mathrm{e}^{\mathrm{i}\mathbf{k}\cdot\mathbf{x}}, \tag{4}$$

where $\mathbf{k} = k_y\mathbf{e}_y = -k\mathbf{e}_y$.

3. Field representations in $\Omega^{\pm}$

This section describes the main ingredients of the semi-analytical model used to study the scattering properties of an infinite grating of circular inclusions coated by a viscoelastic layer embedded in a thin plate. More details on LMST are presented in Appendix A. The formalism considered in [31] for acoustic waves is also adapted here for flexural waves.

The scattered field in both configurations is expanded over plane waves. However, only the discrete set of propagative wavevectors $k_x^\mu\mathbf{e}_x \pm k_y^\mu\mathbf{e}_y$ and evanescent wavevectors $\gamma_x^\mu\mathbf{e}_x \pm \gamma_y^\mu\mathbf{e}_y$ is admissible [44,45] due to the d_x-periodicity of the grating, where the propagative and evanescent Bloch wavenumbers are expressed, respectively, as

$$k_x^\mu = \frac{2\pi\mu}{d_x}, \tag{5}$$

$$\gamma_x^\mu = \frac{2\pi\mu}{d_x}, \tag{6}$$

and $k_y^\mu = \sqrt{k^2 - k_x^{\mu 2}}$ and $\gamma_y^\mu = \sqrt{(ik)^2 - \gamma_x^{\mu 2}}$ with $\mu \in \mathbb{Z}$.

3.1. Transmission problem

The displacement fields w^+ in Ω^+ and w^- in Ω^- are expanded over plane waves in the transmission problem by considering the spatial periodicity as follows:

$$w^+(\mathbf{x}) = \sum_{\mu\in\mathbb{Z}} \delta_{\mu 0}\,\mathrm{e}^{\mathrm{i}k_x^\mu x - \mathrm{i}k_y^\mu(y-(y_0+a))} + R_\mu^p\,\mathrm{e}^{\mathrm{i}k_x^\mu x + \mathrm{i}k_y^\mu(y-(y_0+a))}$$
$$+ R_\mu^e\,\mathrm{e}^{\mathrm{i}\gamma_x^\mu x + \mathrm{i}\gamma_y^\mu(y-(y_0+a))}, \quad \text{with } (x,y)\in\Omega^+, \tag{7a}$$

$$w^-(\mathbf{x}) = \sum_{\mu\in\mathbb{Z}} T_\mu^p\,\mathrm{e}^{\mathrm{i}k_x^\mu x - \mathrm{i}k_y^\mu(y-(y_0-a))} + T_\mu^e\,\mathrm{e}^{\mathrm{i}\gamma_x^\mu x - \mathrm{i}\gamma_y^\mu(y-(y_0-a))}, \quad \text{with } (x,y)\in\Omega^-, \tag{7b}$$

where $\delta_{\mu 0}$ is the Kronecker delta and corresponds to the unitary amplitude of the incident plane waves and R_μ^p, R_μ^e, T_μ^p and T_μ^e are the reflection and transmission coefficients associated with the μ-th Bloch propagative (p) and evanescent (e) waves radiated from the grating in $\Omega^{\pm}$. The expressions of the complex valued coefficients R_μ^p, R_μ^e, T_μ^p and T_μ^e are derived by means of the Green–Kirchhoff Integral Theorem [31] and take the form

$$R_\mu^p = \sum_{n\in\mathbb{Z}} A^0_{\mathrm{H}_n} K^{p+}_{\mu n}\, \mathrm{e}^{-\mathrm{i}k_x^\mu x_0 + \mathrm{i}k_y^\mu a}, \tag{8a}$$

$$R_\mu^e = \sum_{n\in\mathbb{Z}} A^0_{\mathrm{K}_n} K^{e+}_{\mu n}\, \mathrm{e}^{-\mathrm{i}\gamma_x^\mu x_0 + \mathrm{i}\gamma_y^\mu a}, \tag{8b}$$

$$T_\mu^p = \delta_{\mu 0}\, \mathrm{e}^{\mathrm{i}k_x^\mu x - \mathrm{i}k_y^\mu (y-(y_0+a))} + \sum_{n\in\mathbb{Z}} A^0_{\mathrm{H}_n} K^{p-}_{\mu n}\, \mathrm{e}^{-\mathrm{i}k_x^\mu x_0 + \mathrm{i}k_y^\mu y_0}, \tag{8c}$$

$$T_\mu^e = \sum_{n\in\mathbb{Z}} A^0_{\mathrm{K}_n} K^{e-}_{\mu n}\, \mathrm{e}^{-\mathrm{i}\gamma_x^\mu x_0 + \mathrm{i}\gamma_y^\mu y_0}, \tag{8d}$$

where $A^0_{\mathrm{H}_n}$ and $A^0_{\mathrm{K}_n}$ are the scattering coefficients of the circular inclusion Ω^0 determined by means of the boundary conditions at the interface between the inclusion and the surrounding plate, the computation steps of which are detailed in A.5, and

$$K^{p\pm}_{\mu n} = \frac{2(-\mathrm{i})^n}{d_x k_y^\mu}\, \mathrm{e}^{\mathrm{i}\pm n\theta_\mu}, \tag{9a}$$

$$K^{e\pm}_{\mu n} = \frac{\mathrm{i}\pi}{d_x \gamma_y^\mu}\, \mathrm{e}^{\mathrm{i}\pm n\alpha_\mu}, \tag{9b}$$

with $k\,\mathrm{e}^{\mathrm{i}\theta_\mu} = k_x^\mu + \mathrm{i}k_y^\mu$ and $\gamma\,\mathrm{e}^{\mathrm{i}\alpha_\mu} = \gamma_x^\mu + \mathrm{i}\gamma_y^\mu$. The reflectance, transmittance and absorption coefficient α_T of the grating are subsequently evaluated via [46]:

$$|R_T|^2 = \sum_{\mu\in\mathbb{Z}} \frac{\mathrm{Re}(k_y^\mu)}{k_y^0} |R_\mu^p|^2, \tag{10}$$

$$|T_T|^2 = \sum_{\mu\in\mathbb{Z}} \frac{\mathrm{Re}(k_y^\mu)}{k_y^0} |T_\mu^p|^2, \tag{11}$$

$$\alpha_T = 1 - |R_T|^2 - |T_T|^2. \tag{12}$$

3.2. Reflection problem

The interaction of the grating with a plane boundary Γ^p parallel to the grating and located at $y = 0$ is now studied (see Figure 1(a)). This study is possible owing to the expansion of the scattered field w_{sc} upon Bloch waves expressed in Equations (7a) and (7b). A simply supported condition is chosen here in order to analyze the simplest case in which no conversion of wave types from propagative to evanescent, and vice-versa, occurs [47]. The incident wave remains the same as in the previous study and is also expressed by Equation (4). The

half-space Ω^+ is now only considered. The displacement field w^+ in Ω^+ formally reads as the form of Equation (7a). However, the expressions of the reflection coefficients differ from that of Equation (8a) and (8b) due to the presence of the simply supported boundary. The scattering coefficients A_{H_n} and A_{K_n} by the circular inclusion Ω^0 are therefore determined by a slightly different system and read as (details of the calculation are provided in Appendix A.6)

$$R^p_\mu = -\delta_{\mu 0}\,\mathrm{e}^{\mathrm{i}2k^\mu_y(y_0+a)} + \sum_{n\in\mathbb{Z}} A_{\mathrm{H}_n}\,\mathrm{e}^{\mathrm{i}k^\mu_y(y_0+a)}(K^{p+}_{\mu n}\,\mathrm{e}^{-\mathrm{i}k^\mu_x x_0-\mathrm{i}k^\mu_y y_0} - K^{p-}_{\mu n}\,\mathrm{e}^{-\mathrm{i}k^\mu_x x_0+\mathrm{i}k^\mu_y y_0}), \quad (13a)$$

$$R^e_\mu = \sum_{n\in\mathbb{Z}} A_{\mathrm{K}_n}\,\mathrm{e}^{\mathrm{i}\gamma^\mu_y(y_0+a)}(K^{e+}_{\mu n}\,\mathrm{e}^{-\mathrm{i}\gamma^\mu_x x_0-\mathrm{i}\gamma^\mu_y y_0} - K^{e-}_{\mu n}\,\mathrm{e}^{-\mathrm{i}\gamma^\mu_x x_0+\mathrm{i}\gamma^\mu_y y_0}). \quad (13b)$$

The reflectance and absorption coefficient of the grating are thus expressed as

$$|R_R|^2 = \sum_{\mu\in\mathbb{Z}} \frac{\mathrm{Re}(k^\mu_y)}{k^0_y}|R^p_\mu|^2, \quad (14)$$

$$\alpha_R = 1 - |R_R|^2. \quad (15)$$

3.3. Critical coupling conditions

3.3.1. Transmission problem

The absorption efficiency of the grating is studied by analyzing its scattering properties. In the study case of transmission in far-field ($y \to \pm\infty$) with identical inclusions, the scattering process is symmetric and reciprocal. The scattering of the system can thus be represented by means of the scattering matrix **S** or *S*-matrix of the propagative waves with the following form:

$$\mathbf{S} = \begin{bmatrix} T_T & R_T \\ R_T & T_T \end{bmatrix}, \quad y \to \pm\infty. \quad (16)$$

The complex eigenvalues $\psi_{1,2}$ of **S** can therefore be expressed as $\psi_1 = T_T + R_T$ and $\psi_2 = T_T - R_T$. These two eigenvalues correspond to the reflection coefficient of two independent reflection problems created by a virtual boundary condition placed at y_0 with either a Neumann ($\partial w/\partial y = 0$) or a Dirichlet ($w = 0$) condition, respectively [48,49]. The first eigenvalue, $\psi_1 = R_s$ corresponds to the reflection coefficient of the symmetric sub-problem as Neumann boundary condition selects the modes with symmetric profiles [49]. Analogously, the second one, $\psi_2 = R_a$ corresponds to the anti-symmetric sub-problem [49]. Then, the absorption coefficient of the propagative waves for each sub-problem can be defined as

$$\alpha_s = 1 - |R_s|^2, \quad (17)$$

$$\alpha_a = 1 - |R_a|^2. \quad (18)$$

Finally, the total absorption coefficient of the original scattering problem in the transmission problem reads as

$$\alpha_T = \frac{\alpha_s + \alpha_a}{2}. \quad (19)$$

The configuration in which the incident wave is totally absorbed corresponds, therefore, to that where $\alpha_s = \alpha_a = 1$ and so $|R_s|^2 = |R_a|^2 = 0$. In other words, it corresponds to the case in which the two eigenvalues of the original scattering matrix of the transmission problem are zero. However, the grating analyzed here at the piston-like (monopolar) mode of the inclusions, i.e. only the symmetric part of the problem can be perfectly absorbed. Therefore, the optimal absorption of the system in the transmission problem is limited to 0.5.

3.3.2. Reflection problem

The reflection coefficient R_R represents the scattering of the system in the case of a reflection problem, since no wave is transmitted through the grating. Thus, R_R corresponds directly to both the S-matrix and its associated eigenvalue ($\psi = R_R$), and the absorption coefficient of the scattering problem reads as $\alpha_R = 1 - |R_R|^2$. In this case, the configuration of total absorption of the incident wave by the scatterer corresponds to that where $R_R = 0$.

4. Results

The two scattering problems, depicted in Figure 1, are now considered in the particular case where the incident field w_{inc} is a propagative plane wave of unitary amplitude along the direction $-\mathbf{e}_y$. An aluminium plate of thickness $h = 5$ mm is considered with $E = 70$ GPa, $\rho = 2800\,\text{kg.m}^{-3}$, and $\nu = 0.3$, for all the problems. The viscoelastic coating used in the resonators is a tape of thickness $h_l = 0.3$ mm and properties $E_l = 0.5$ GPa, $\rho_l = 950\,\text{kg.m}^{-3}$, $\nu_l = 0.3$, and $\eta_l = 0.7$. Although the loss factor should be frequency-dependent, it is assumed that this factor is constant over the analyzed frequency range. This approximation has previously been considered in [17] and provided good agreements between the analytical and experimental results. More complex viscoelastic models, like Zener or generalized Maxwell-based model, or Karjanson's formula could also be considered. Nevertheless, those are for highly dissipative materials, with quality factors lower than 50. They also make the problem more complex, which is not relevant in the context of this work considering the frequency range of interest and the materials under study. It is also considered that the inclusions have a radius of $a = 7.5$ cm, the added mass has a thickness $h_m = 5$ mm and the grating has a periodicity of $d_x = 20$ cm.

This section focuses on the reflection and transmission of waves in the far-field, ($y \to \pm\infty$), i.e. on the propagative waves that carry the energy. The expansion of the displacement fields upon Bloch waves is truncated such that $\mu \in [-20 : 20]$. The lattice sums S^{H}_{n-q} and S^{K}_{n-q} used to compute the scattered displacement fields (see Appendix A.2 for more details) are expanded upon 2000 terms, which ensures the convergence. The results are validated against those simulated by 3D FEM models implemented with the solid mechanics module in COMSOL Multiphysics®. The geometry of the FEM model is composed of a single unit cell of the circular inclusion grating, in which the periodicity along $\mathbf{e}_x$ is simulated using Floquet conditions and the infinite length along $\mathbf{e}_y$ with Perfectly Matched Layers (PML) (see Figure 2). The simply supported condition used in the reflection model is simulated by imposing a zero displacement along $\mathbf{e}_z$ at the corresponding boundary, while the incident plane wave in both problems is created by imposing a harmonic load along a line parallel to the grating axis.

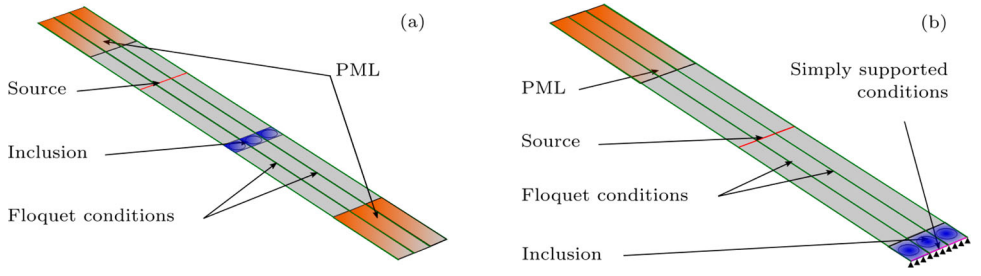

Figure 2. (a) 3D FEM model of three unit cells of the infinite grating of inclusions used in COMSOL software to numerically compute $|R_T|^2$, $|T_T|^2$ and α_T in the transmission problem. The periodicity along $\mathbf{e}_x$ is simulated using Floquet conditions and the infinite length along $\mathbf{e}_y$ with Perfectly Matched Layers (PML). (b) 3D FEM model of three unit cells of the infinite grating of inclusions used in COMSOL software to numerically compute $|R_T|^2$ and α_T in the reflection problem. The PML from one side imposes the semi-infinite length of the system while on the other side, a simply supported boundary condition is considered to create the reflection problem.

4.1. Transmission problem

The inclusion thickness h_0 and the added mass radius r_m are first optimized to reach the maximum absorption coefficient at the inclusion fundamental frequency (piston-like or monopolar mode). The maximum absorption is found for $h_0 = 0.3$ mm and $r_m = 3$ cm. Figure 3(a) depicts $|R_T|^2$, $|T_T|^2$ and $\alpha_T = 1 - |R_T|^2 - |T_T|^2$ using both the LMST and FEM models for this configuration, which are found to be in good agreement. The absorption coefficient α_T reaches 0.5 at $f = 70.7$ Hz as shown in Figure 3(a). This frequency corresponds approximately to the resonance frequency of the first axisymmetric mode of the isolated resonators, which was evaluated afterwards at $f_0 = 69$ Hz. This slight difference in the resonance frequency can be explained by a weak coupling between the resonator in the grating. The monopolar nature of the mode is also testified by the displacement field snapshot depicted in Figure 3(b), where a maximum of displacement is clearly visible close to the center of the inclusions. This pattern of displacement clearly shows that the resonant mode of the system at the first axisymmetric mode is symmetric with respect to the $\mathbf{e}_z$ axis. Thus, as discussed in Section 3.3.1, the transmission problem can only be half critically coupled by making use of a single symmetric mode [17], and the maximum of absorption obtained here is only 0.5.

The results are also interpreted by making use of the Argand diagram, in which the real and imaginary parts of a physical parameter are plotted. In this case, the Argand diagram of the two eigenvalues $\psi_1 = |R_T + T_T|^2$ and $\psi_2 = |R_T - T_T|^2$ of the problem is plotted from 50 to 100 Hz as shown in solid blue lines in Figures 3(c) and 3(d), respectively. Note that each frequency corresponds to a point in this diagram, therefore, the analysis of a range of frequencies produces a line. Both eigenvalues ψ_1 and ψ_2 follow a circular trajectory in each diagram. The sense of the increasing frequencies is shown with arrows. It is clearly seen that only the trajectory of ψ_1 passes through the origin of the diagram as shown with the purple point in Figure 3(c). The frequency corresponding to this point is $f = 70.7$ Hz and corresponds to the frequency of maximal absorption, meaning that $\psi_1 = 0$ and $\psi_2 \neq 0$ at the resonance frequency. As a consequence, the perfect absorption is only obtained for the symmetric sub-problem at $f = 70.7$ Hz and the maximum of absorption of the general problem is limited to 0.5.

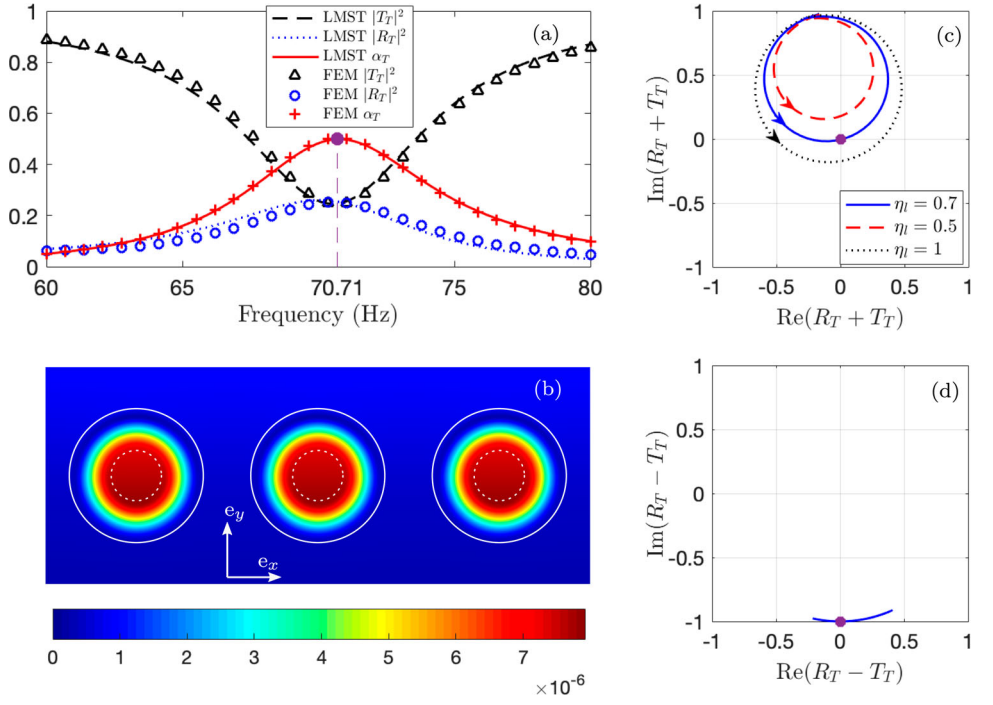

Figure 3. (a) Representation of $|R_T|^2$,$|T_T|^2$ and α_T around the first eigenfrequency of the critically coupled resonators in the transmission problem. (b) Displacement field obtained in the FEM model in the vicinity of the inclusions along $\mathbf{e}_z$ at $\mathrm{Re}(f) = 70.7$ Hz in the transmission problem. The boundaries of the resonators and the masses are outlined in white solid and dashed lines, respectively. (c) Argand diagram of $(R_T + T_T)$ from 50 to 100 Hz for $\eta_l = 0.7$ (solid line), $\eta_l = 1$ (dashed line) and $\eta_l = 0.5$ (dotted line). The purple point corresponds to the maximum of absorption at $f = 70.7$ Hz. (d) Argand diagram of $(R_T - T_T)$ from 50 to 100 Hz. The point corresponds to the maximum of absorption at $f = 70.7$ Hz.

Such a kind of representation provides information about the effect of the losses on the system. The Argand diagram of ψ_1 is then depicted in dashed line in Figure 3(c) for the case in which an excess of losses is introduced by the coating layer ($\eta_l = 0.5$). The trajectory of ψ_1 remains circular, but no longer passes through the origin due to the excess of losses. As a consequence, ψ_1 does not equal 0 and the maximum of absorption is under 0.5. Note also that in this case, the origin of the diagram is located outside the circular trajectory of ψ_1. On the contrary, case where the system lacks losses as shown in black dotted line in Figure 3(c), the circle still does not pass through the origin leading also to an absorption lower than 0.5. However, the lack of losses is characterized in this case by a location of the origin that is inside the circle of ψ_1.

4.2. Reflection problem

The grating obtained in the transmission problem is now bounded by imposing a simply supported boundary at a distance y_0, converting the previous transmission problem to a reflection one. As discussed in Section 3.3.2, perfect absorption can be obtained in this configuration. The only free parameter that remains in this problem is the distance between the

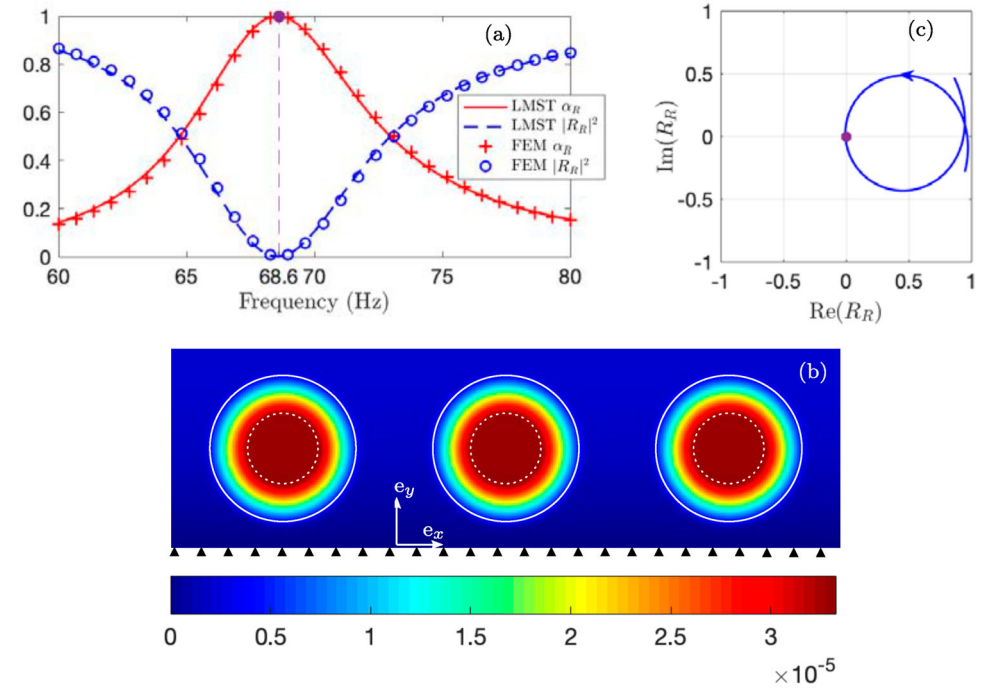

Figure 4. (a) Representation of $|R_R|^2$ and α_R around the first eigenfrequency of the critically coupled resonators in the reflection problem. The point corresponds to the maximum of absorption at $f = 68.6$ Hz. (b) Displacement field obtained in the FEM model in the vicinity of the inclusions along $\mathbf{e}_z$ at $\mathrm{Re}(f) = 68.6$ Hz in the reflection problem. The boundaries of the resonators and the masses are outlined in white solid and dashed lines, respectively. (c) Argand diagram of R_R from 50 to 100 Hz. The point corresponds to the maximum of absorption at $f = 68.6$ Hz.

simply supported boundary and the grating. By doing a parametric analysis, it is found that the perfect absorption is reached for $y_0 = 8.95$ cm.

Figure 4(a) depicts $|R_R|^2$ and α_R of the grating resonator located at $x_0 = 10$ cm and $y_0 = 8.95$ cm in unit cells of width $d_x = 20$ cm. An absorption $\alpha_R \simeq 1$ at $f = 68.6$ Hz is noticed, meaning that the incident plane wave is totally absorbed by the grating of resonators at this specific frequency. In order to interpret these results, the Argand diagram is used once again for the reflection coefficient. Its trajectory in the Argand diagram from 50 to 100 Hz in Figure 4(c) also illustrates the perfect absorption of the incident wave. The trajectory of R_R possesses a circular shape and passes through the origin of the diagram at $f = 68.6$ Hz, meaning that $|R_R| \simeq 0$ at this particular frequency. The perfect absorption is therefore obtained at $f = 68.6$ Hz and $\alpha_R \simeq 1$. This means that the critical coupling condition is fulfilled for this configuration at this frequency. The displacement response inside the resonators at $f = 68.6$ Hz takes again the typical form of that of a first axi-symmetric mode as shown in Figure 4(b).

4.3. Optimization of absorption by making use of local resonances and the periodicity of the grating: platonic crystal

The results presented in previous subsections highlight the adaptability of the critical coupling method to optimize the absorption of LRMs for flexural waves in 2D transmission and

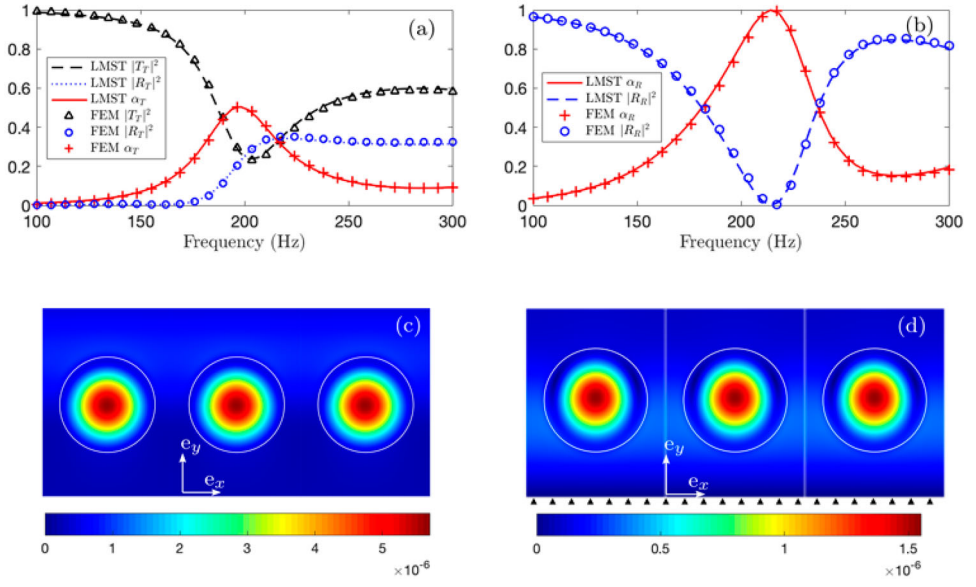

Figure 5. (a) Representation of $|R_T|^2$, $|T_T|^2$ and α_T around the Bragg frequency of the platonic crystal in the transmission problem. (b) Displacement field obtained in the FEM model in the vicinity of the inclusions along $\mathbf{e}_z$ at $\mathrm{Re}(f) = 196$ Hz in the reflection problem. The boundaries of the resonators are outlined in white solid lines. (c) Representation of $|R_R|^2$ and α_T around the Bragg frequency of the platonic crystal in the reflection problem. The resonators are outlined in white solid lines. (d) Displacement field obtained in the FEM model in the vicinity of the inclusions along $\mathbf{e}_z$ at $\mathrm{Re}(f) = 217$ Hz in the reflection problem.

reflection problems. This was made possible by using a geometry of inclusion that ensures its first resonance at a frequency which is three times smaller than the Bragg frequency of the grating, allowing a decoupling between the resonances and the Bragg scattering. This section aims to show that such results can also be obtained at higher frequencies in the case of platonic crystals, and where the first inclusion resonance f_0 is close to the Bragg frequency f_{bragg} of the grating. The two same scattering problems are considered here, except that the inclusions have no more an added mass in their center but consist of homogeneous circular reductions of the plate thickness, on top of which a viscoelastic coating is placed. All the properties remain the same as before except the inclusion thickness $h_0 = 0.84$ mm and radius $a = 10$ cm, the coating thickness $h_l = 0.7$ mm and loss factor $\eta_l = 2$, and the size of the unit cell of the grating $d_x = 24$ cm and d_y. These properties provide a first inclusion resonance at $f_0 = 184.9$ Hz and a Bragg frequency $f_{bragg} = 206.3$ Hz. The properties of the coating layer are also chosen to optimize the absorption of the system for both scattering problems. The absorption coefficient α_T reaches again 0.5 at $f = 196$ Hz in the transmission problem as shown in Figure 5(a), whereas $\alpha_R \simeq 1$ at $f = 214$ Hz in the reflection problem.

5. Conclusions

The absorption of a propagative flexural incident plane wave by an infinite grating of circular resonators in 2D thin plates is studied. The absorbing efficiency of this system is analyzed by means of the reflection, transmission and absorption coefficients using the

LMST for both the reflection and the transmission problems. In the transmission problem, the physical conditions imply only one type of symmetry of the resonant modes, and limit the absorption of the grating to 50%. Two strategies could be considered to obtain a perfection absorption. The first one would be to use degenerate resonators with two types of symmetry at the same frequency. The second strategy would be to break the symmetry of the resonators in order to treat the full problem with a single type of symmetry of the resonance mode [14]. One way to break the symmetry of the resonators would be to consider a stack of parallel gratings. The resonance of a stack of parallel gratings in plates has already been studied for the transmission problem by Haslinger et al.[7,8]. In particular, Haslinger et al. brought to light the Elasto Dynamically Inhibited Transmission (EDIT) by tuning and coinciding local symmetric and anti-symmetric resonances of a stack of three parallel gratings of rigid pins with a shifted middle grating. This filtering effect is related to the Electromagnetically Induced Transparency (EIT) in optic fields, and is characterized by peaks of transparency due to the coherent interferences between the two resonators. Although resonances have been studied in [7,8], the type of resonance obtained differs from that presented in this work, in that the resonances in [7,8] are Fabry–Perot resonances and not local resonances due to resonant scatterers. Therefore, these resonances are not obtained from the geometry of the inclusions itself but from the spatial configuration of the gratings. The wavelength related to the frequency range of interest in [7,8] is then of the same order as the spatial configuration of the gratings. Note also that the analysis by Haslinger et al. only focused on the lossless case, i.e. without inherent losses in the system. No absorption phenomena have therefore been analyzed. In the reflection problem, perfect absorption is possible. The results of this work highlight the adaptability of the critical coupling method applied to flexural waves for problems in thin plates. The resonators used here, the type of incident wave and the boundary conditions have been chosen as simple as possible and give the key features for future designs of 2D subwavelength perfect absorbers for flexural waves.

Disclosure statement

No potential conflict of interest was reported by the author(s).

Funding

This work has been funded by the RFI Le Mans Acoustique (Région Pays de la Loire) within the framework of the MetaplaQ project. This article is based upon work from COST action DENORMS CA 15125, supported by COST (European Cooperation in Science and Technology). This work was partly supported by the project HYPERMETA funded under the program Étoiles Montantes de la Région Pays de la Loire and by the project eTNAA ANR-17-CE08-0035-01 (projet ANR 2017-2021). The authors also acknowledge support from the Spanish Ministry of Economy and Innovation (MINECO) and European Union FEDER through project PID2019-109175GB-C22.

References

[1] Ross D, Ungar EL, Kerwin EM. Damping of plate flexural vibrations by means of viscoelastic laminae. Struct Damping. 1960;49–87.

[2] Snowdon JC. Dynamic vibration absorbers that have increased effectiveness. J Eng Ind. 1974;96(3):940–945.

[3] Morvaridi M, Carta G, Brun M. Platonic crystal with low-frequency locally-resonant spiral structures: wave trapping, transmission amplification, shielding and edge waves. J Mech Phys Solids. 2018;121:496–516.
[4] Zhou X, Wang L. Opening complete band gaps in two dimensional locally resonant phononic crystals. J Phys Chem Solids. 2018;116:174–179.
[5] Cai L-W, Hambric SA. Multiple scattering of flexural waves on thin plates. J Vib Acoust. 2016;138(1).
[6] Gao P, Climente A, Sánchez-Dehesa J, et al. Theoretical study of platonic crystals with periodically structured n-beam resonators. J Appl Phys. 2018;123(9):091707.
[7] Haslinger SG, Movchan NV, Movchan AB, et al. Transmission, trapping and filtering of waves in periodically constrained elastic plates. Proc R Soc A Math Phys Eng Sci. 2012;468(2137):76–93.
[8] Haslinger SG, Movchan AB, Movchan NV, et al. Symmetry and resonant modes in platonic grating stacks. Waves Random Complex Media. 2014;24(2):126–148.
[9] Lee WM, Chen JT. Scattering of flexural wave in a thin plate with multiple circular inclusions by using the multipole method. Int J Mech Sci. 2011;53(8):617–627.
[10] Movchan NV, McPhedran RC, Movchan AB, et al. Wave scattering by platonic grating stacks. Proc R Soc A Math Phys Eng Sci. 2009;465(2111):3383–3400.
[11] Parnell WJ, Martin PA. Multiple scattering of flexural waves by random configurations of inclusions in thin plates. Wave Motion. 2011;48(2):161–175.
[12] Zhu R, Liu XN, Hu GK, et al. Microstructural designs of plate-type elastic metamaterial and their potential applications: a review. Int J Smart Nano Mater. 2015;6(1):14–40.
[13] Cai M, Painter O, Vahala KJ. Observation of critical coupling in a fiber taper to a silica-microsphere whispering-gallery mode system. Phys Rev Lett. 2000;85(1):74.
[14] Jiménez N, Romero-García V, Pagneux V, et al. Rainbow-trapping absorbers: broadband, perfect and asymmetric sound absorption by subwavelength panels for transmission problems. Sci Rep. 2017;7(1):13595.
[15] Romero-García V, Theocharis G, Richoux O, et al. Use of complex frequency plane to design broadband and sub-wavelength absorbers. J Acoust Soc Am. 2016;139(6):3395–3403.
[16] Xu Y, Li Y, Lee RK, et al. Scattering-theory analysis of waveguide-resonator coupling. Phys Rev E. 2000;62(5):7389.
[17] Leng J, Gautier F, Pelat A, et al. Limits of flexural wave absorption by open lossy resonators: reflection and transmission problems. New J Phys. 2019;21(5):053003.
[18] Duan Y, Luo J, Wang G, et al. Theoretical requirements for broadband perfect absorption of acoustic waves by ultra-thin elastic meta-films. Sci Rep. 2015;5:12139.
[19] Fang N, Xi D, Xu J, et al. Ultrasonic metamaterials with negative modulus. Nat Mater. 2006;5(6):452.
[20] Groby J-P, Pommier R, Aurégan Y. Use of slow sound to design perfect and broadband passive sound absorbing materials. J Acoust Soc Am. 2016;139:1660–1671.
[21] Liu Z, Zhang X, Mao Y, et al. Locally resonant sonic materials. Science. 2000;289(5485):1734–1736.
[22] Skelton EA, Craster RV, Colombi A, et al. The multi-physics metawedge: graded arrays on fluid-loaded elastic plates and the mechanical analogues of rainbow trapping and mode conversion. New J Phys. 2018;20:053017.
[23] Wei P, Croënne C, Tak Chu S, et al. Symmetrical and anti-symmetrical coherent perfect absorption for acoustic waves. Appl Phys Lett. 2014;104(12):121902.
[24] Bliokh KY, Bliokh YP, Freilikher V, et al. Colloquium: unusual resonators: plasmonics, metamaterials, and random media. Rev Mod Phys. 2008;80(4):1201.
[25] Yariv A. Universal relations for coupling of optical power between microresonators and dielectric waveguides. Electron Lett. 2000;36(4):321–322.
[26] Cao L, Yang Z, S-W Fan YXu. Flexural wave absorption by lossy gradient elastic metasurface. J Mech Phys Solids. 2020;143:104052.
[27] Thorpe JI, Numata K, Livas J. Laser frequency stabilization and control through offset sideband locking to optical cavities. Opt Express. 2008;16(20):15980–15990.

[28] Botten LC, McPhedran RC, de Sterke CM, et al. From multipole methods to photonic crystal device modeling. In: Yasumoto K, editor. Electromagnetic theory and applications for photonic crystals. Boca Raton, FL: CRC Press; 2005. p. 47–122.
[29] Martin PA. Multiple scattering: interaction of time-harmonic waves with N obstacles. New-York (NY): Cambridge University Press; 2006.
[30] Sainidou R, Stefanou N, Psarobas IE, et al. A layer-multiple-scattering method for phononic crystals and heterostructures of such. Comput Phys Commun. 2005;166(3):197–240.
[31] Schwan L, Groby J-P. Introduction to multiple scattering theory. In: Romero-García V, & Hladky-Hennion A-C, editors. Fundamentals and applications of acoustic metamaterials: from seismic to radio frequency (Vol. 1). New Jersey: John Wiley & Sons; 2019. p. 143–182.
[32] Yasumoto K. Electromagnetic theory and applications for photonic crystals. Boca Raton (FL): CRC Press; 2006.
[33] Watson GN. A treatise on the theory of Bessel functions. New York (NY): Cambridge University Press; 1995.
[34] Abramowitz M, Stegun IA. Handbook of mathematical functions with formulas, graphs, and mathematical table. US Department of Commerce; 1965. (National Bureau of standards applied mathematics series, 55).
[35] Linton CM. Schlömilch series that arise in diffraction theory and their efficient computation. J Phys A Math Gen. 2006;39(13):3325.
[36] McPhedran RC, Nicorovici NA, Botten LC, et al. Green's function, lattice sums and Rayleigh's identity for a dynamic scattering problem. In: Papanicolaou G, editor. Wave propagation in complex media. New York (NY): Springer; 1998. p. 155–186.
[37] Twersky V. Elementary function representations of Schlömilch series. Arch Ration Mech Anal. 1961;8(1):323–332.
[38] Evans DV, Porter R. Penetration of flexural waves through a periodically constrained thin elastic plate in vacuo and floating on water. J Eng Math. 2007;58(1-4):317–337.
[39] Movchan AB, Movchan NV, McPhedran RC. Bloch–Floquet bending waves in perforated thin plates. Proc R Soc A: Math Phys Eng Sci. 2007;463(2086):2505–2518.
[40] Poulton CG, McPhedran RC, Movchan NV, et al. Convergence properties and flat bands in platonic crystal band structures using the multipole formulation. Waves Random Complex Media. 2010;20(4):702–716.
[41] Smith MJA, McPhedran RC, Meylan MH. Double Dirac cones at $k = 0$ in pinned platonic crystals. Waves Random Complex Media. 2014;24(1):35–54.
[42] Smith MJA, McPhedran RC, Poulton CG, et al. Negative refraction and dispersion phenomena in platonic clusters. Waves Random Complex Media. 2012;22(4):435–458.
[43] Leissa AW. Vibration of plates. Technical report, Ohio State Univ Columbus, 1969.
[44] Bloch F. Über die quantenmechanik der elektronen in kristallgittern. Z Phys. 1929;52(7–8):555–600.
[45] Floquet G. Sur les équations différentielles linéaires à coefficients périodiques. Ann Sci Éc Norm Supér. 1883;12:47–88.
[46] Groby J-P, Wirgin A, Ogam E. Acoustic response of a periodic distribution of macroscopic inclusions within a rigid frame porous plate. Waves Random Complex Media. 2008;18(3):409–433.
[47] Cuenca J, Gautier F, Simon L. Harmonic Green's functions for flexural waves in semi-infinite plates with arbitrary boundary conditions and high-frequency approximation for convex polygonal plates. J Sound Vib. 2012;331(6):1426–1440.
[48] Merkel A, Theocharis G, Richoux O, et al. Control of acoustic absorption in one-dimensional scattering by resonant scatterers. Appl Phys Lett. 2015;107(24):244102.
[49] Romero-García V, Jiménez N, Groby JP, et al. Perfect absorption in mirror-symmetric acoustic metascreens; 2020. arXiv:2007.08393.
[50] Abramowitz M. Handbook of mathematical functions with formulas, graphs, and mathematical tables. NBS:1964. p. 232. (Applied mathematics series, 55).
[51] Cai LW, Sánchez-Dehesa J. Acoustical scattering by radially stratified scatterers. J Acoust Soc Am. 2008;124(5):2715–2726.

[52] Norris AN, Vemula C. Scattering of flexural waves on thin plates. J Sound Vib. 1995;181(1):115–125.
[53] Barber PW, Hill SC. Light scattering by particles: computational methods (Vol. 2). New Jersey: World Scientific; 1990.

Appendices

Appendix 1. Viscoelastic losses in the resonator: the RKU model for plates

Each resonator of the grating is covered by a thin absorbing layer of thickness h_l, the losses of which are considered frequency independent. The complex Young Modulus of the absorbing layer is $E_l(1-\mathrm{i}\eta_l)$, where η_l is its loss factor. Each resonator can also be discretized in two homogeneous axisymmetric layers, one containing the added mass and denoted by (m), and another without mass denoted (0) (see Figure 1(b)). Using the RKU model for a plate [1], each layer of the resonators is modeled as a single composite layer with a given effective wave number k_i^p written as

$$k_i^p = \left(\frac{12\omega^2\rho(1-\nu^2)}{Eh_i^2} \left[\frac{1+\rho_r^p h_{i,r}^p}{(1-\mathrm{i}\eta)+1-\mathrm{i}\eta_l)h_{i,r}^p E_r^p \alpha_i^p} \right] \right)^{1/4}, \tag{A1}$$

where $i = 0$ or m, and the indices 0, m and l stand for the parameters of the uncoated layer without and with the added mass and of the absorbing layer, respectively, $\rho_r^p = \frac{\rho_l}{\rho}, h_{i,r}^p = \frac{h_l}{h_i}, E_r^p = \frac{E_l}{E}$ and $\alpha_i^p = 3 + 6h_{i,r}^p + 4{h_{i,r}^p}^2$. The flexural bending stiffness D_i^p for each layer can then be written as

$$D_i^p = \frac{h_i^3}{12(1-\nu^2)} E\left[(1+h_{i,r}^p E_r^p \alpha_i^p) - \mathrm{i}\left(\eta + \nu_l h_{i,r} E_r^p \alpha_i^p\right)\right]. \tag{A2}$$

The mass density of the composite layers corresponds to the mean value of the mass density of the uncoated layer and the absorbing material, such that

$$\rho_i^p = \frac{\rho h_i + \rho_l h_l}{h_i^p}, \tag{A3}$$

where $h_i^p = h_i + h_l$, and the Poisson coefficient of the composite is considered the same as the uncoated resonator's:

$$\nu_0^p = \nu. \tag{A4}$$

Appendix 2. Computation of the scattering coefficients

This section aims at detailing the computation steps to determine the scattering coefficients of each inclusion in the two scattering problems described in Section 2.1. To do that, a polar coordinate system $(O^j, \mathbf{e}_r^j, \mathbf{e}_\theta^j)$ is attached to the center of each circular inclusion Ω_j (see Figure A6). The position vector according to the coordinate systems attached to each inclusion Ω_j is written as $\mathbf{r}^j = r^j\mathbf{e}_r^j + \theta^j\mathbf{e}_\theta^j$.

A.1 Quasi-periodicity

The displacement field in the infinite plate can be expressed as the sum of the incident plane wave w_{inc} and the scattered field w_{sc} by the grating. The latter is the sum of the scattered fields w_{sc}^j by each inclusion Ω^j, thus the total displacement field reads as

$$w = w_{\mathrm{inc}} + w_{\mathrm{sc}} = w_{\mathrm{inc}}(\mathbf{x}) + \sum_{j\in\mathbb{Z}} w_{\mathrm{sc}}^j(\mathbf{r}^j). \tag{A5}$$

Each scattered field w_{sc}^j is first expanded upon outgoing propagating and evanescent waves in its own cylindrical coordinate system using Hankel functions of the first kind and Bessel functions of the

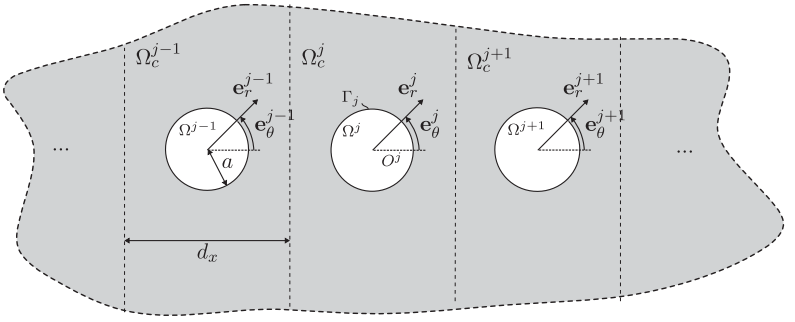

Figure A6. Sketch of the configuration of the scattering problem by an infinite grating of circular inclusions embedded in a thin plate with the polar coordinate systems.

second kind:

$$w_{\mathrm{sc}}^j(\mathbf{r}^j) = \sum_{n\in\mathbb{Z}} [A_{\mathrm{H},n}^j \mathrm{H}_n^{(1)}(kr^j) + A_{\mathrm{K},n}^j \mathrm{K}_n(kr^j)]\, \mathrm{e}^{\mathrm{i}n\theta^j}, \tag{A6}$$

where $A_{\mathrm{H},n}^j$ and $A_{\mathrm{K},n}^j$ are the propagative and evanescent scattering coefficients of Ω^j, respectively. Due to the quasi-periodicity of the grating along $\mathbf{e}_x$, the number of scattering coefficients to determine can be reduced by exploiting the Floquet–Bloch condition:

$$A_{\mathrm{H},n}^j = A_{\mathrm{H},n}^0\, \mathrm{e}^{\mathrm{i}jk_x d_x} \quad j \in \mathbb{Z}, \tag{A7}$$

$$A_{\mathrm{K},n}^j = A_{\mathrm{K},n}^0\, \mathrm{e}^{\mathrm{i}jk_x d_x} \quad j \in \mathbb{Z}. \tag{A8}$$

As a consequence of Equations (A7)–(A8), it is sufficient to determine the scattering coefficients of one inclusion Ω^j to solve the problem. Moreover, Equation (4) can be expanded upon Bessel functions using the Jacobi–Anger expansion [50] such that

$$w_{\mathrm{inc}}(r,\theta) = \sum_{n\in\mathbb{Z}} [A_{\mathrm{J},n}^{\mathrm{inc}} \mathrm{J}_n(kr^j) + A_{\mathrm{I},n}^{\mathrm{inc}} \mathrm{I}_n(kr^j)]\, \mathrm{e}^{\mathrm{i}n\theta^j}, \tag{A9}$$

where $A_{\mathrm{J},n}^{\mathrm{inc}} = \mathrm{i}^n\, \mathrm{e}^{-\mathrm{i}n\theta_{\mathrm{inc}}}$ and $A_{\mathrm{I},n}^{\mathrm{inc}} = 0$ are the incident amplitudes and $\theta_{\mathrm{inc}} = -\pi/2$.

A.2 Lattice sum

The scattering coefficients of the inclusion Ω^0 are now determined. The total scattered displacement field w_{sc} therefore takes the following form:

$$w_{\mathrm{sc}}(\mathbf{r}^j) = \sum_{j\in\mathbb{Z}} \sum_{n\in\mathbb{Z}} [A_{\mathrm{H},n}^0 \mathrm{H}_n^{(1)}(kr^j) + A_{\mathrm{K},n}^0 \mathrm{K}_n(kr^j)]\, \mathrm{e}^{\mathrm{i}n\theta^j}. \tag{A10}$$

Graf's addition [34] theorem is then used to express all the fields scattered by each inclusion Ω^j, with $j \in \mathbb{Z}^*$, according to the local polar coordinate system $(O^0, \mathbf{e}_r^0, \mathbf{e}_\theta^0)$ attached to Ω^0. The total scattered displacement field w_{sc} can be expressed in the vicinity of Ω^0 as

$$\begin{aligned} w_{\mathrm{sc}}(\mathbf{r}^0) = &\sum_{n\in\mathbb{Z}} [A_{\mathrm{H},n}^0 \mathrm{H}_n^{(1)}(kr^0) + A_{\mathrm{K},n}^0 \mathrm{K}_n(kr^0)]\, \mathrm{e}^{\mathrm{i}n\theta^0} \\ &+ \sum_{n\in\mathbb{Z}} \sum_{q\in\mathbb{Z}} [A_{\mathrm{H},q}^0 S_{n-q}^{\mathrm{H}} \mathrm{J}_n(kr^0)\, \mathrm{e}^{\mathrm{i}n\theta^0} + A_{\mathrm{K},q}^0 S_{n-q}^{\mathrm{K}} \mathrm{I}_n(kr^0)]\, \mathrm{e}^{\mathrm{i}n\theta^0}, \quad r^0 < d_x - a \cap \Omega_c^0, \end{aligned} \tag{A11}$$

where S_{n-q}^{H} and S_{n-q}^{K} are written as

$$S_{n-q}^{\mathrm{H}} = \sum_{j>0} \mathrm{H}_{n-q}^{(1)}(kjd)(\mathrm{e}^{\mathrm{i}jk_x} + (-1)^{n-q}\, \mathrm{e}^{-\mathrm{i}jk_x}), \tag{A12}$$

$$S^{\mathrm{K}}_{n-q} = \sum_{j>0} \mathrm{K}_{n-q}(kjd)((-1)^n\,\mathrm{e}^{-\mathrm{i}jk_x} + (-1)^q\,\mathrm{e}^{\mathrm{i}jk_x}). \tag{A13}$$

In particular, Equation (A12) is known as the lattice sum or the Schlömilch series. Such a serie arises naturally in scattering problems where the scatterer is an infinite periodic structure and accounts for the contribution of the fields scattered by Ω^j, where $j \in \mathbb{Z}^*$, to the near-field close to Ω^0 [35]. The form of the series as written in Equation (A12) is not suitable for numerical computation due to its very slow convergence. However, it can be transformed into another expression which is amenable for computation [35,37]. As $\mathrm{H}^{(1)}_{q-n}(kjd) = (-1)^{n-q}\mathrm{H}^{(1)}_{n-q}(kjd)$, $S^{\mathrm{H}}_{n-q} = S^{\mathrm{H}}_{q-n}$. Furthermore, the transformation of this serie takes several forms whether the order $|n-q|$ is even, odd or 0 [35,37]. If $n-q=0$:

$$S^{\mathrm{H}}_0 = -1 - \frac{2\mathrm{i}}{\pi}\left(C + ln\left(\frac{kd}{4\pi}\right)\right) + \frac{2}{kd\sin\Phi_0} + {\sum_{m\in\mathbb{Z}}}'\left(\frac{2}{kd\sin\Phi_0}+\right), \tag{A14}$$

where $\Phi_m = \arccos(\cos\theta_{\mathrm{inc}} + \frac{2m\pi}{kd})$ and C is the Euler constant.

If $|n-q|$ is even,

$$S^{\mathrm{H}}_{n-q} = 2 - (-1)^N \sum_{m\in\mathbb{Z}} \frac{\mathrm{e}^{\mathrm{i}(n-q)\,\mathrm{sign}(m)\Phi_m}}{kd\sin\Phi_m} + 2\mathrm{i}\lambda_N, \tag{A15}$$

where $N = (n-q)/2$, $\mathrm{sign}(m)$ is the sign of m with the convention $\mathrm{sign}(0) = +1$ and

$$\lambda_N = \frac{1}{2\pi}\sum_{m=0}^{N} \frac{(-1)^m 2^{2m}(N+m-1)!}{(2m)!(N-m)!}\left(\frac{2\pi}{kd}\right)^{2m} B_{2m}(0), \tag{A16}$$

with B_m the Bernoulli polynomial.

If $|n-q|$ is odd,

$$S^{\mathrm{H}}_{n-q} = 2 - (-1)^M \mathrm{i} \sum_{m\in\mathbb{Z}} \frac{\mathrm{e}^{\mathrm{i}(2M-1)\,\mathrm{sign}(m)\Phi_m}}{kd\sin\Phi_m} + 2\lambda_M, \tag{A17}$$

where $M = (n-q+1)/2$ and

$$\lambda_M = \frac{1}{\pi}\sum_{m=0}^{M-1} \frac{(-1)^m 2^{2m}(M+m-1)!}{(2m+1)!(M-m-1)!}\left(\frac{2\pi}{kd}\right)^{2m+1} B_{2m+1}(0). \tag{A18}$$

Note that this slow convergence concerns only S^{H}_{n-q} in the lossless case and not S^{K}_{n-q}, since $\mathrm{K}_n(x)$ is exponentially decaying with the increasing argument x. Using the appropriate expression of the Schlömilch serie, the total displacement field in the polar coordinate system $(O^0, \mathbf{e}^0_r, \mathbf{e}^0_\theta)$ takes the following form in the vicinity of Ω^0 ($r^0 < d_x - a \cap \Omega^0_c$):

$$\begin{aligned} w(\mathbf{r}^0) = \sum_{n\in\mathbb{Z}} & [A^0_{\mathrm{H},n}\mathrm{H}^{(1)}_n(kr^0) + A^0_{\mathrm{K},n}\mathrm{K}_n(kr^0) \\ & + (A_{\mathrm{J},n}{}^{\mathrm{inc},0} + \mathcal{A}^0_{\mathrm{H},n})\mathrm{J}_n(kr^0) + \mathcal{A}^0_{\mathrm{K},n}\mathrm{I}_n(kr^0)]\,\mathrm{e}^{\mathrm{i}n\theta^0}, \end{aligned} \tag{A19}$$

where

$$\mathcal{A}^0_{\mathrm{H},n} = \sum_{q\in\mathbb{Z}} A^0_{\mathrm{H},q}S^{\mathrm{H}}_{n-q} \quad \text{and} \quad \mathcal{A}^0_{\mathrm{K},n} = \sum_{q\in\mathbb{Z}} A^0_{\mathrm{K},q}S^{\mathrm{K}}_{n-q}. \tag{A20}$$

A.3 Flexural field inside the inclusions

A multilayer scattering approach is adopted to characterize the flexural field inside each inclusion [51]. This approach gives the relation between the converging and diverging amplitudes at the interface inside the inclusions between the two circular coated layers (m) and (0). The flexural field w_0^p of layer (0) is therefore described as the sum of the field w_0^{p-} transmitted by the surrounded plate with the field w_0^{p+} scattered by layer (m):

$$w_0^p = w_0^{p-} + w_0^{p+} = \sum_{n\in\mathbb{Z}} A_{\mathrm{J},n}^{(0)} \mathrm{J}_n(k_0^p r) + A_{\mathrm{I},n}^{(0)} \mathrm{I}_n(k_0^p r) + A_{\mathrm{H},n}^{(0)} \mathrm{H}_n^{(1)}(k_0^p r) + A_{\mathrm{K},n}^{(0)} \mathrm{K}_n(k_0^p r). \tag{A21}$$

The notation $^-$ describes a converging propagation of the fields towards the center of the inclusion and $^+$ denotes a diverging propagation. Due to the singularity of $\mathrm{H}_n(z)$ and $\mathrm{K}_n(z)$ when $z = 0$, the field of layer (m) has to be described as

$$w_m^p = \sum_{n\in\mathbb{Z}} A_{\mathrm{J},n}^{(m)} \mathrm{J}_n(k_m^p r) + A_{\mathrm{I},n}^{(m)} \mathrm{I}_n(k_m^p r). \tag{A22}$$

A.4 Reflection coefficient of isolated Ω^0

By using the notations $\mathbf{W}_{\mathbf{n,j}}^- = \begin{pmatrix} A_{\mathrm{J},n}^{(j)} \\ A_{\mathrm{I},n}^{(j)} \end{pmatrix}$, $j = 0$ or m, $\mathbf{W}_{\mathbf{n,0}}^+ = \begin{pmatrix} A_{\mathrm{H},0}^{(j)} \\ A_{\mathrm{K},0}^{(j)} \end{pmatrix}$, $\mathbf{W}_{\mathbf{n}}^- = \begin{pmatrix} A_{\mathrm{J},n}^{\mathrm{inc}} \\ A_{\mathrm{I},n}^{\mathrm{inc}} \end{pmatrix}$ and $\mathbf{W}_{\mathbf{n}}^+ = \begin{pmatrix} A_{\mathrm{H},n}^{0} \\ A_{\mathrm{K},0}^{0} \end{pmatrix}$, the scattering relations at the interface between layer (0) and layer (m) and between layer (0) and the surrounding plate at the order n can be written in the case of a single inclusion as

$$\begin{cases} \mathbf{W}_{\mathbf{n,m}}^- = \mathbf{T}_{\mathbf{n,m}}^- \mathbf{W}_{\mathbf{n,0}}^-, \\ \mathbf{W}_{\mathbf{n,0}}^+ = \mathbf{R}_{\mathbf{n,m}}^+ \mathbf{W}_{\mathbf{n,0}}^-, \\ \mathbf{W}_{\mathbf{n,0}}^- = \mathbf{T}_{\mathbf{n,0}}^- \mathbf{W}_{\mathbf{n}}^-, \\ \mathbf{W}_{\mathbf{n}}^+ = \mathbf{R}_{\mathbf{n,0}}^+ \mathbf{W}_{\mathbf{n}}^- + \mathbf{T}_{\mathbf{n,0}}^+ \mathbf{W}_{\mathbf{n,0}}^+, \end{cases} \tag{A23}$$

where $\mathbf{T}_{\mathbf{n,m}}^-$ and $\mathbf{T}_{\mathbf{n,m}}^+$ are, respectively, the converging and diverging transmission coefficients at the order n at the interface, and $\mathbf{R}_{\mathbf{n,m}}^-$ and $\mathbf{R}_{\mathbf{n,m}}^+$ the converging and diverging reflection coefficients at the order n, respectively. $\mathbf{T}_{\mathbf{n,m}}^-$, $\mathbf{T}_{\mathbf{n,m}}^+$, $\mathbf{R}_{\mathbf{n,m}}^-$ and $\mathbf{R}_{\mathbf{n,m}}^+$ are obtained by writing the boundary conditions at each interfaces, i.e. the continuity of displacement, displacement normal derivative, bending moment and (Kirchhoff) shear force, and by considering two types of incidence: converging incidence and diverging incidence [51]. Assuming that all the scattering coefficients are known, it might be possible to express the amplitude of all the converging and diverging fields as a function of the incident field outside the scatterer and its scattering coefficients. In particular, $\mathbf{W}_{\mathbf{n}}^+ = \begin{pmatrix} R_{11}^n \\ R_{12}^n \end{pmatrix}$ in the case of a propagative incident wave of unit amplitude as expressed in Equation (A9) and $\mathbf{W}_{\mathbf{n}}^+ = \begin{pmatrix} R_{21}^n \\ R_{22}^n \end{pmatrix}$ in the case of a pure evanescent incident wave with $A_{\mathrm{J},n}^{\mathrm{inc}} = 0$ and $A_{\mathrm{I},n}^{\mathrm{inc}} = \mathrm{i}^n$, where $R^n = \begin{bmatrix} R_{11}^n & R_{12}^n \\ R_{21}^n & R_{22}^n \end{bmatrix}$ is the reflection coefficient of a single inclusion.

A.5 Boundary conditions at Γ_0 for the transmission problem

The scattering coefficients of Ω^0 are determined by means of the boundary conditions at the interface Γ_0 between the scatterer and the surrounding plate, i.e. the continuity of displacement, displacement normal derivative, bending moment and (Kirchhoff) shear force [52], and by considering the scattered amplitudes by the other inclusions of Equation (A20) in the incident field propagating toward Ω^0. In the case where the scattered field is expanded upon N orders of Hankel functions and modified Bessel functions of the second kind ($n \in [-N; N]$, $N \in \mathbb{Z}$), the scattering coefficients are determined from the

boundary conditions by solving the following system:

$$\begin{cases} A^0_{\mathrm{H}_{-N}} - R^{-N}_{11}\sum_{q\in\mathbb{Z}} A^0_{\mathrm{H}_q} S^{\mathrm{H}}_{-N-q} - R^{-N}_{12}\sum_{q\in\mathbb{Z}} A^0_{\mathrm{K}_q} S^{\mathrm{K}}_{-N-q} = R^{-N}_{11} A^{\mathrm{inc},0}_{\mathrm{J},-N} \\ A^0_{\mathrm{K}_{-N}} - R^{-N}_{21}\sum_{q\in\mathbb{Z}} A^0_{\mathrm{H}_q} S^{\mathrm{H}}_{-N-q} - R^{-N}_{22}\sum_{q\in\mathbb{Z}} A^0_{\mathrm{K}_q} S^{\mathrm{K}}_{-N-q} = R^{-N}_{21} A^{\mathrm{inc},0}_{\mathrm{J},-N} \\ \vdots \\ A^0_{\mathrm{H}_0} - R^0_{11}\sum_{q\in\mathbb{Z}} A^0_{\mathrm{H}_q} S^{\mathrm{H}}_{0-q} - R^0_{12}\sum_{q\in\mathbb{Z}} A^0_{\mathrm{K}_q} S^{\mathrm{K}}_{0-q} = R^0_{11} A^{\mathrm{inc},0}_{\mathrm{J},0} \\ A^0_{\mathrm{K}_0} - R^0_{21}\sum_{q\in\mathbb{Z}} A^0_{\mathrm{H}_q} S^{\mathrm{H}}_{0-q} - R^0_{22}\sum_{q\in\mathbb{Z}} A^0_{\mathrm{K}_q} S^{\mathrm{K}}_{0-q} = R^0_{21} A^{\mathrm{inc},0}_{\mathrm{J},0} \\ \vdots \\ A^0_{\mathrm{H}_N} - R^N_{11}\sum_{q\in\mathbb{Z}} A^0_{\mathrm{H}_q} S^{\mathrm{H}}_{N-q} - R^N_{12}\sum_{q\in\mathbb{Z}} A^0_{\mathrm{K}_q} S^{\mathrm{K}}_{N-q} = R^N_{11} A^{\mathrm{inc},0}_{\mathrm{J},N} \\ A^0_{\mathrm{K}_N} - R^N_{21}\sum_{q\in\mathbb{Z}} A^0_{\mathrm{H}_q} S^{\mathrm{H}}_{N-q} - R^N_{22}\sum_{q\in\mathbb{Z}} A^0_{\mathrm{K}_q} S^{\mathrm{K}}_{N-q} = R^N_{21} A^{\mathrm{inc},0}_{\mathrm{J},N} \end{cases}. \tag{A24}$$

The sums are truncated in practice to $n \in [-N; N]$ by using the following numerical recipe [53]:

$$N = \mathrm{floor}(4.05(ka)^{1/3} + ka) + 10 \tag{A25}$$

to ensure their convergence. Note that this truncation concerns only the Hankel functions of the first kind and the Bessel functions of the second kind in the scattered field, and that the lattice sum which runs over the spatial repetition of the unit cell is evaluated independently of this truncation.

A.6 Boundary conditions at Γ_0 for the reflection problem

The displacement field inside the unit cell Ω^0_c can be expressed as the sum of the scattered field inside Ω_c (i.e. for $0 < y < y_0 - a$) and the reflected waves at the boundary Γ^+ such that

$$\begin{aligned} w^0_c(\mathbf{x}) = &\sum_{\mu\in\mathbb{Z}} f^{p+}_\mu \,\mathrm{e}^{\mathrm{i}k^\mu_x x + \mathrm{i}k^\mu_y y} + f^{p-}_\mu \,\mathrm{e}^{\mathrm{i}k^\mu_x x - \mathrm{i}k^\mu_y y} + f^{e+}_\mu \,\mathrm{e}^{\mathrm{i}\gamma^\mu_x x + \mathrm{i}\gamma^\mu_y y} + f^{e-}_\mu \,\mathrm{e}^{\mathrm{i}\gamma^\mu_x x - \mathrm{i}\gamma^\mu_y y} \\ &+ \sum_{n\in\mathbb{Z}} A^0_{\mathrm{H}_n} K^{p\pm}_{\mu n} \,\mathrm{e}^{-\mathrm{i}k^\mu_x x_0 \pm \mathrm{i}k^\mu_y a} \,\mathrm{e}^{\mathrm{i}k^\mu_x x + \pm \mathrm{i}k^\mu_y (y-(y_0+a))} \\ &+ A^0_{\mathrm{K}_n} K^{e\pm}_{\mu n} \,\mathrm{e}^{-\mathrm{i}\gamma^\mu_x x_0 \mp \mathrm{i}\gamma^\mu_y a} \,\mathrm{e}^{\mathrm{i}\gamma^\mu_x x \pm \mathrm{i}\gamma^\mu_y (y-(y_0+a))}, \end{aligned} \tag{A26}$$

where the upper signs are taken when $y \in \Omega^+$ ($y > y_0 + a$) and the lower signs when $0 < y < y_0 - a$. f^{p+}_μ and f^{p-}_μ account for the amplitudes of the ingoing and outgoing propagative Bloch waves in Ω^0_c, respectively, whereas f^{e+}_μ and f^{e-}_μ correspond to the amplitudes of the ingoing and outgoing evanescent Bloch waves in Ω^0_c, respectively. The scattering coefficients in w^+ as well as the waves' amplitudes of w^0_c are determined by means of the boundary conditions at Γ^+ and Γ^p. The boundary conditions at Γ^p and the continuity conditions at Γ^+ imply

$$\begin{cases} \displaystyle\int_0^{d_x} w^0_c \,\mathrm{e}^{-\mathrm{i}k^\nu_x x}\,\mathrm{d}x = \int_0^{d_x} w^+ \,\mathrm{e}^{-\mathrm{i}k^\nu_x x}\,\mathrm{d}x \\ \displaystyle\int_0^{d_x} \frac{\partial w^0_c}{\partial y} \,\mathrm{e}^{-\mathrm{i}k^\nu_x x}\,\mathrm{d}x = \int_0^{d_x} \frac{\partial w^+}{\partial y} \,\mathrm{e}^{-\mathrm{i}k^\nu_x x}\,\mathrm{d}x \end{cases}, \quad y \in \Gamma^+, \tag{A27}$$

and

$$\begin{cases} \displaystyle\int_0^{d_x} w^0_c \,\mathrm{e}^{-\mathrm{i}k^\nu_x x}\,\mathrm{d}x = 0 \\ \displaystyle\int_0^{d_x} \frac{\partial^2 w^0_c}{\partial y^2} \,\mathrm{e}^{-\mathrm{i}k^\nu_x x}\,\mathrm{d}x = 0 \end{cases}, \quad y \in \Gamma^p. \tag{A28}$$

Applying the boundary conditions at Γ^+, Γ^p and making use of the orthogonality relation $\int_0^{d_x} \mathrm{e}^{\mathrm{i}k_x^\mu x}\,\mathrm{e}^{-\mathrm{i}k_x^\nu x}\,\mathrm{d}x = 2\pi\, d_x \delta_{\nu\mu}$, the amplitudes f_μ^{p+}, f_μ^{p-}, f_μ^{e+} and f_μ^{e-}, and the propagative and evanescent reflection coefficients R_μ^p and R_μ^e can be expressed as

$$f_\mu^{p+} = -\delta_{q0}\,\mathrm{e}^{\mathrm{i}k_y^\mu(y_0+a)} - \sum_{n\in\mathbb{Z}} A_{\mathrm{H}_n} K_{\mu n}^{p-}\,\mathrm{e}^{-\mathrm{i}k_x^\mu x_0 + \mathrm{i}k_y^\mu y_0}, \tag{A29a}$$

$$f_\mu^{p-} = \delta_{\mu 0}\,\mathrm{e}^{\mathrm{i}k_y^\mu(y_0+a)}, \tag{A29b}$$

$$f_\mu^{e+} = -\sum_{n\in\mathbb{Z}} A_{\mathrm{K}_n} K_{\mu n}^{e-}\,\mathrm{e}^{-\mathrm{i}\gamma_x^\mu x_0 + \mathrm{i}\gamma_y^\mu y_0}, f_\mu^{e-} = 0, \tag{A29c}$$

$$R_\mu^p = -\delta_{\mu 0}\,\mathrm{e}^{\mathrm{i}2k_y^\mu(y_0+a)} + \sum_{n\in\mathbb{Z}} A_{\mathrm{H}_n}\,\mathrm{e}^{\mathrm{i}k_y^\mu(y_0+a)}(K_{\mu n}^{p+}\,\mathrm{e}^{-\mathrm{i}k_x^\mu x_0 - \mathrm{i}k_y^\mu y_0} - K_{\mu n}^{p-}\,\mathrm{e}^{-\mathrm{i}k_x^\mu x_0 + \mathrm{i}k_y^\mu y_0}), \tag{A29d}$$

$$R_\mu^e = \sum_{n\in\mathbb{Z}} A_{\mathrm{K}_n}\,\mathrm{e}^{\mathrm{i}\gamma_y^\mu(y_0+a)}(K_{\mu n}^{e+}\,\mathrm{e}^{-\mathrm{i}\gamma_x^\mu x_0 - \mathrm{i}\gamma_y^\mu y_0} - K_{\mu n}^{e-}\,\mathrm{e}^{-\mathrm{i}k_x^\mu x_0 + \mathrm{i}\gamma_y^\mu y_0}). \tag{A29e}$$

f_μ^{p-} and f_μ^{e-} account therefore for the incident wave amplitudes in Ω_c^0, whereas f_μ^{p+} and f_μ^{e+} accounts for the reflection at Γ^p of the incident wave and the scattered field by Ω^0. The scattering coefficients A_{H_n} and A_{K_n} of Ω^0 are again determined by means of the boundary conditions at Γ_0. However, it requires beforehand to expand the exponential terms of w_c^0 upon Bessel functions in the coordinate system $(O^0, \mathbf{e}_r^0, \mathbf{e}_\theta^0)$ by using the Jacobi-Anger expansion, such that

$$f_\mu^{p+}\,\mathrm{e}^{\mathrm{i}k_x^\mu x + \mathrm{i}k_y^\mu y} = \sum_{n\in\mathbb{Z}} F_{\mu n}^{p+}\mathrm{J}_n(kr^0)\,\mathrm{e}^{\mathrm{i}n\theta^0}, \tag{A30a}$$

$$f_\mu^{e+}\,\mathrm{e}^{\mathrm{i}\gamma_x^\mu x + \mathrm{i}\gamma_y^\mu y} = \sum_{n\in\mathbb{Z}} F_{\mu n}^{e+}\mathrm{I}_n(kr^0)\,\mathrm{e}^{\mathrm{i}n\theta^0} \tag{A30b}$$

with

$$F_{\mu n}^{p+} = \left(-\delta_{\mu 0}\,\mathrm{e}^{\mathrm{i}k_y^\mu(y_0+a)} - \sum_{m\in\mathbb{Z}} A_{\mathrm{H}_m}^0 K_{\mu m}^{p-}\,\mathrm{e}^{-\mathrm{i}k_x^\mu x_0 + \mathrm{i}k_y^\mu y_0}\right)\mathrm{i}^n\,\mathrm{e}^{-\mathrm{i}n\theta_\mu}\,\mathrm{e}^{\mathrm{i}k_x^\mu x_0 + \mathrm{i}k_y^\mu y_0}, \tag{A31a}$$

$$F_{\mu n}^{e+} = -\sum_{m\in\mathbb{Z}} A_{\mathrm{K}_m}^0 K_{\mu m}^{e-}\,\mathrm{e}^{-\mathrm{i}\gamma_x^\mu x_0 + \mathrm{i}\gamma_y^\mu y_0}(-1)^n\,\mathrm{e}^{-\mathrm{i}n\alpha_\mu}\,\mathrm{e}^{\mathrm{i}\gamma_x^\mu x_0 + \mathrm{i}\gamma_y^\mu y_0}. \tag{A31b}$$

Hence, if the scattered field is expanded upon N orders of Hankel functions and modified Bessel functions of the second kind, the scattering coefficients are determined from the boundary conditions at

Γ_0 by solving the following system:

$$\begin{cases} A^0_{\mathrm{H}_{-N}} - R^{-N}_{11}\mathcal{S}^H_{-N} - R^{-N}_{12}\mathcal{S}^K_{-N} = R^{-N}_{11}\left(A^{\mathrm{inc},0}_{\mathrm{J},-N} - \sum_{\mu\in\mathbb{Z}} \delta_{\mu 0}\, \mathrm{e}^{\mathrm{i}k_y^\mu (y_0+a)} \mathrm{i}^{-N}\, \mathrm{e}^{\mathrm{i}N\theta_\mu}\, \mathrm{e}^{\mathrm{i}k_x^\mu x_0 + \mathrm{i}k_y^\mu y_0}\right) \\ A^0_{\mathrm{K}_{-N}} - R^{-N}_{21}\mathcal{S}^H_{-N} - R^{-N}_{22}\mathcal{S}^K_{-N} = R^{-N}_{21}\left(A^{\mathrm{inc},0}_{\mathrm{J},-N} - \sum_{\mu\in\mathbb{Z}} \delta_{\mu 0}\, \mathrm{e}^{\mathrm{i}k_y^\mu (y_0+a)} \mathrm{i}^{-N}\, \mathrm{e}^{\mathrm{i}N\theta_\mu}\, \mathrm{e}^{\mathrm{i}k_x^\mu x_0 + \mathrm{i}k_y^\mu y_0}\right) \\ \vdots \\ A^0_{\mathrm{H}_0} - R^0_{11}\mathcal{S}^H_0 - R^0_{12}\mathcal{S}^K_0 = R^0_{11}\left(A^{\mathrm{inc},0}_{\mathrm{J},0} - \sum_{\mu\in\mathbb{Z}} \delta_{\mu 0}\, \mathrm{e}^{\mathrm{i}k_y^\mu (y_0+a)}\, \mathrm{e}^{\mathrm{i}k_x^\mu x_0 + \mathrm{i}k_y^\mu y_0}\right) \\ A^0_{\mathrm{K}_0} - R^0_{21}\mathcal{S}^H_0 - R^0_{22}\mathcal{S}^K_0 = R^0_{21}\left(A^{\mathrm{inc},0}_{\mathrm{J},0} - \sum_{\mu\in\mathbb{Z}} \delta_{\mu 0}\, \mathrm{e}^{\mathrm{i}k_y^\mu (y_0+a)}\, \mathrm{e}^{\mathrm{i}k_x^\mu x_0 + \mathrm{i}k_y^\mu y_0}\right) \\ \vdots \\ A^0_{\mathrm{H}_N} - R^N_{11}\mathcal{S}^H_N - R^N_{12}\mathcal{S}^K_N = R^N_{11}\left(A^{\mathrm{inc},0}_{\mathrm{J},N} - \sum_{\mu\in\mathbb{Z}} \delta_{\mu 0}\, \mathrm{e}^{\mathrm{i}k_y^\mu (y_0+a)} \mathrm{i}^{N}\, \mathrm{e}^{-\mathrm{i}N\theta_\mu}\, \mathrm{e}^{\mathrm{i}k_x^\mu x_0 + \mathrm{i}k_y^\mu y_0}\right) \\ A^0_{\mathrm{K}_N} - R^N_{21}\mathcal{S}^H_N - R^N_{22}\mathcal{S}^K_N = R^N_{21}\left(A^{\mathrm{inc},0}_{\mathrm{J},N} - \sum_{\mu\in\mathbb{Z}} \delta_{\mu 0}\, \mathrm{e}^{\mathrm{i}k_y^\mu (y_0+a)} \mathrm{i}^{N}\, \mathrm{e}^{-\mathrm{i}N\theta_\mu}\, \mathrm{e}^{\mathrm{i}k_x^\mu x_0 + \mathrm{i}k_y^\mu y_0}\right) \end{cases} \tag{A32}$$

with

$$\mathcal{S}^H_n = \sum_{q\in\mathbb{Z}} A^0_{\mathrm{H}_q}\left(S^{\mathrm{H}}_{n-q} - \sum_{\mu\in\mathbb{Z}} \mathrm{e}^{\mathrm{i}2k_y^\mu y_0} K_{\mu q}{}^{p-} \mathrm{i}^n\, \mathrm{e}^{-\mathrm{i}n\theta_\mu}\right), \tag{A33a}$$

$$\mathcal{S}^K_n = \sum_{q\in\mathbb{Z}} A^0_{\mathrm{K}_q}\left(S^{\mathrm{K}}_{n-q} - \sum_{\mu\in\mathbb{Z}} \mathrm{e}^{\mathrm{i}2\gamma_y^\mu y_0} K^{e-}_{\mu q}(-1)^n\, \mathrm{e}^{-\mathrm{i}n\theta_\mu}\right). \tag{A33b}$$